



HAL
open science

Human GLP1R variants affecting GLP1R cell surface expression are associated with impaired glucose control and increased adiposity

Wenwen Gao, Lei Liu, Eunna Huh, Florence Gbahou, Erika Cecon, Masaya Oshima, Ludivine Houzé, Panagiotis Katsonis, Alan Hegron, Zhiran Fan, et al.

► To cite this version:

Wenwen Gao, Lei Liu, Eunna Huh, Florence Gbahou, Erika Cecon, et al.. Human GLP1R variants affecting GLP1R cell surface expression are associated with impaired glucose control and increased adiposity. *Nature Metabolism*, 2023, 10.1038/s42255-023-00889-6 . hal-04233247

HAL Id: hal-04233247

<https://hal.science/hal-04233247v1>

Submitted on 23 Nov 2023

HAL is a multi-disciplinary open access archive for the deposit and dissemination of scientific research documents, whether they are published or not. The documents may come from teaching and research institutions in France or abroad, or from public or private research centers.

L'archive ouverte pluridisciplinaire **HAL**, est destinée au dépôt et à la diffusion de documents scientifiques de niveau recherche, publiés ou non, émanant des établissements d'enseignement et de recherche français ou étrangers, des laboratoires publics ou privés.



Distributed under a Creative Commons Attribution 4.0 International License

1 **Human *GLP1R* variants affecting *GLP1R* cell surface expression are associated with**
2 **impaired glucose control and increased adiposity**

3 Wenwen Gao^{1,2}, Lei Liu^{1,3}, Eunna Huh⁴, Florence Gbahou¹, Erika Cecon¹, Masaya Oishma¹,
4 Ludivine Houzé¹, Panagiotis Katsonis⁴, Alan Hegron^{1,5,6}, Zhiran Fan³, Guofei Hou³, Guillaume
5 Charpentier⁷, Mathilde Boissel⁸, Mehdi Derhourhi⁸, Michel Marre^{9,10}, Beverley Balkau¹¹,
6 Philippe Froguel^{8,12}, Raphael Scharfmann¹, Olivier Lichtarge^{4,13}, Julie Dam¹, Amélie
7 Bonnefond^{8,12,14}, Jianfeng Liu^{3,14,*}, Ralf Jockers^{1,14,15,*}

8
9 ¹ Université Paris Cité, Institut Cochin, INSERM, CNRS, 75014 Paris, France

10 ² State Key Laboratory for Diagnosis and Treatment of Severe Zoonotic Infectious Diseases,
11 Key Laboratory for Zoonosis Research of the Ministry of Education, Institute of Zoonosis, and
12 College of Veterinary Medicine, Jilin University, Changchun 130062, China

13 ³ Cellular Signaling Laboratory, International Research Center for Sensory Biology and
14 Technology of MOST, Key Laboratory of Molecular Biophysics of Ministry of Education,
15 School of Life Science and Technology, Huazhong University of Science and Technology,
16 Wuhan, China

17 ⁴ Department of Pharmacology and Chemical Biology, Baylor College of Medicine, Houston,
18 TX 77030, United States of America

19 ⁵ Institute for Research in Immunology and Cancer, University of Montreal, Montreal, QC,
20 Canada

21 ⁶ Department of biochemistry and Molecular Medicine, University of Montreal, QC, Canada

22 ⁷ CERITD (Centre d'Étude et de Recherche pour l'Intensification du Traitement du Diabète),
23 Evry, France

24 ⁸ University of Lille, Inserm UMR1283, CNRS UMR8199, European Genomic Institute for
25 Diabetes (EGID), Institut Pasteur de Lille, Lille University Hospital, Lille, 59000, France

26 ⁹ Institut Necker-Enfants Malades, INSERM, Université de Paris, Paris, France

27 ¹⁰ Clinique Ambroise Paré, Neuilly-sur-Seine, France

28 ¹¹ Inserm U1018, Center for Research in Epidemiology and Population Health, Villejuif, France

29 // University Paris-Saclay, University Paris-Sud, Villejuif, France

30 ¹² Department of Metabolism, Imperial College London, London, W12 0NN, United Kingdom

31 ¹³ Department of Molecular and Human Genetics, Baylor College of Medicine, Houston, TX
32 77030, United States of America

33 ¹⁴ Co-senior authors

34 ¹⁵ Lead contact

35 * Correspondence: ralf.jockers@inserm.fr (R.J.), jfliu@mail.hust.edu.cn (J.L.)

36
37 **Running title:** Functional diversity of *GLP1R* variants

38

39

40

41 **Abstract**

42 The glucagon-like peptide 1 receptor (GLP1R) is a major drug target with several agonists being
43 prescribed in patients with type 2 diabetes (T2D) and obesity^{1,2}. The impact of genetic variability
44 of *GLP1R* on receptor function and its association with metabolic traits are unclear with
45 conflicting reports. Here, we performed a functional profiling of 60 *GLP1R* variants across four
46 signaling pathways and revealed an unexpected diversity of phenotypes ranging from defective
47 cell surface expression to complete or pathway-specific gain- (GoF) and loss-of-functions (LoF).
48 The defective insulin secretion of *GLP1R* LoF variants was rescued by allosteric GLP1R ligands
49 or high concentrations of exendin-4/**semaglutide** in INS-1 823/3 cells. Genetic association studies
50 in 200K participants from the UK Biobank show that impaired GLP1R cell surface expression
51 contributes to poor glucose control and increased adiposity with increased HbA1c, BMI and
52 diastolic blood pressure. This study defines impaired GLP1R cell surface expression as a risk
53 factor for T2D- and obesity-associated traits and provides potential treatment options for *GLP1R*
54 LoF variant carriers.

55

56 **MAIN**

57 While GLP1R³ is a major T2D and obesity drug target, the consequences of *GLP1R* variants on
58 receptor function and metabolic traits have remained poorly defined¹. Conflicting results have
59 been reported for frequent variants, including *GLP1R* LOF variants that are not associated with
60 metabolic diseases^{4,5,6} and causality with disease risk was difficult to establish as these
61 variants were in linkage disequilibrium with other genes. Here, we performed large-scale
62 functional genetics of rare *GLP1R* variants enabling putative causality. Among the 132 *GLP1R*
63 variants available in the ExAC browser in 2016, we selected 34 rare missense *GLP1R* variants
64 *i.* which are predicted to be of moderate to high impact based on their evolutionary action (EA)

65 scores^{7,8}, *ii.* for which literature data was available on the functional consequences of alanine
66 mutations⁹, *iii.* which were located in transmembrane and intracellular domains, known to be
67 important for receptor activation and signal transduction (Fig. 1a, Extended Data Fig. 1a and
68 Supplementary Table 1). In parallel, we sequenced *GLP1R* in 8,672 participants from the
69 RaDiO study¹⁰. Among 46 detected missense variants, we selected 25 rare variants and a
70 common one encoding p.A316T because of their high predicted functional impact (Fig. 1a,
71 Extended Data Fig. 1b and Supplementary Table 1). In total, 60 *GLP1R* variants were selected
72 for functional analyses (Fig. 1b).

73 We first determined the abundance of wild-type (WT) and each mutant *GLP1R* at the cell surface
74 in HEK293T cells which do not endogenously express *GLP1R*, and in rat insulinoma INS-1 823/3
75 (*Glp1r* KO) cells deleted of its endogenous *Glp1r* gene¹¹. **Transfection of WT *GLP1R* with a N-**
76 **terminal SNAP-flag-tag resulted in expression levels similar to endogenous *GLP1R* levels found**
77 **in mouse pancreatic islets¹² (Extended Data Fig. 2a-d). Similar results were obtained with non-**
78 **tagged WT *GLP1R* (Extended Data Fig. 2e).** In HEK293T cells, total expression of 22 mutants
79 was significantly lower than WT *GLP1R* (Fig. 1c (color code)). For a subset of mutants,
80 trafficking to the cell surface was in addition significantly affected resulting in 31 variants with
81 significantly reduced surface expression (Fig. 1c (size of bubbles) and Supplementary Table 2a).
82 In INS-1 823/3 (*Glp1r* KO) cells total and surface expression was detectable for all mutants
83 except for p.N320Y and p.I400R (Extended Data Fig. 2f and Supplementary Table 2b). Surface
84 levels matched well in both cell types with occasional deviations for some variants but without
85 any systematic trend towards higher or lower expression in either cell system (Fig. 1d). Defects
86 in receptor trafficking and total expression contributed both to impaired surface expression
87 (Extended Data Fig. 2g,h). Collectively, 22 out of 60 mutants showed significantly reduced cell
88 surface expression in both INS-1 823/3 (*Glp1r* KO) and HEK293T cells.

89 We next established the signaling profile of WT GLP1R and 60 mutants on four signaling
90 pathways (cAMP accumulation, Ca²⁺ mobilization, ERK activation, and β-arrestin 2 (β-arr2)
91 recruitment) in HEK293T cells. No spontaneous receptor activity was observed in the absence
92 of ligand for any pathway for WT GLP1R (Extended Data Fig. 3a-d, f) and the mutants (data not
93 shown). Ex-4 concentration-response curves were generated for the different signaling pathways
94 (Extended Data Fig. 3a-f). To account for differences in cell surface expression levels of GLP1R
95 mutants, we determined the correlation between GLP1R cell surface expression and E_{max} and
96 EC₅₀ values for Ex-4 at different WT GLP1R expression levels (Extended Data Figs. 4a-c and 5)
97 and we performed experiments with expression-matched WT GLP1R (Extended Data Fig. 4d-
98 g). EC₅₀ values were unaffected by the surface expression (Extended Data Figs. 4c and 5c,f,i)
99 and E_{max} values correlated positively with surface expression with a saturation observed for the
100 cAMP pathway at 10 ± 3 % cell surface expression (Extended Data Figs. 4b and 5b,e,h).

101 For the cAMP pathway LoF and GoF variants were observed (Fig. 2 and Extended Data Fig. 6
102 and Supplementary Table 3a). Most LoF mutants can be explained by impaired cell surface
103 expression impacting either EC₅₀ or E_{max} (Extended Data Fig. 4h-k). Interestingly, p.R380C
104 shows normal surface expression but the most severe loss in Ex-4 affinity of all variants (1.5
105 logs; IC₅₀=400 nM) (Fig. 2b and Extended Data Fig. 7). GoF mutants show increased E_{max} values
106 despite normal surface expression. Ca²⁺ mobilization is affected in 2/3 of the studied GLP1R
107 mutants with both LoF and GoF in E_{max} (Fig. 2 and Extended Data Fig. 6 and Supplementary
108 Table 3b). Twenty-seven mutants showed significantly impaired ERK1/2 activation and one
109 mutant (p.S258L) increased ERK1/2 activation (Fig. 2 and Extended Data Fig. 6 and
110 Supplementary Table 3c). The β-arr2 pathway represents the pathway for which most of the
111 mutants are affected with diminished EC₅₀ and/or E_{max} (Fig. 2 and Extended Data Fig. 6 and
112 Supplementary Table 3d). GoF was not observed for this pathway. Based on all these functional
113 analyses we grouped the mutants into eight categories: those with severely impaired cell surface

114 expression (less than 10 ± 3 %), those with all four or two or three pathways impaired, those with
115 specific defects only in β -arr2 recruitment or ERK1/2 signaling, those exhibiting a gain-of-
116 function (GoF) in cAMP or Ca^{2+} signaling, and those similar to WT GLP1R (Fig. 2a-h and
117 [Extended Data Fig. 6a-h](#)).

118 To further evaluate the overall signaling efficiencies of each mutant, we determined their
119 transduction coefficient $\log(\tau/K_a)$, and compared the values of the WT receptor and each mutant
120 by subtracting the corresponding transduction coefficient and expressed it as $\Delta\log(\tau/K_a)$
121 ([Supplementary Table 3a-d](#)). We then plotted radial graphs containing $\Delta\log(\tau/K_a)$ together with
122 E_{\max} values for all pathways to generate a visible signaling signature for each mutant (Fig. 3 and
123 [Extended Data Fig. 6](#)). When excluding the mutants with severely impaired cell surface
124 expression, the cAMP pathway turned out to be the most affected pathway, with eight mutants
125 displaying $\Delta\log(\tau/K_a)$ values of up to -3.16, which is significantly different from zero, the
126 reference value ([Supplementary Table 3a](#)), followed by β -arr2 recruitment ([Supplementary Table](#)
127 [3d](#)) with seven mutants with modest $\Delta\log(\tau/K_a)$ values (between -1.00 and -1.54). Only three and
128 zero mutants showed statistically significant $\Delta\log(\tau/K_a)$ values for Ca^{2+} mobilization
129 ([Supplementary Table 3b](#)) and ERK1/2 activation ([Supplementary Table 3c](#)), respectively.

130 Interestingly, some of the variants showed signaling bias. Five variants encoding p.R227C,
131 p.Y291C, p.R310Q, p.I357F and p.E408G ([Extended Data Fig. 6](#)) were G protein-biased with
132 loss of β -arr2 recruitment but activation of the Gs/cAMP pathway and the Gq/11/ Ca^{2+} pathway
133 ([Supplementary Table 3b](#)). Among these, p.E408G showed even GoF for Ca^{2+} mobilization and
134 p.Y291C for both Ca^{2+} mobilization and cAMP production. None of the mutants were biased
135 towards β -arr2. Three variants encoding p.H173P, p.R190Q ([Extended Data Fig. 6](#)) and p.R380C
136 ([Fig. 2b](#)) were strictly Gs/cAMP biased, as activation of all other pathways were undetectable.

137 Another remarkable finding of our study was that, for many mutants, GoF or LoF was not a
138 general feature of the mutant but was restricted to specific signaling pathways, leading to

139 complex and different signaling signatures for each variant. In some cases, GoF and LoF
140 phenotypes were observed for the same mutants, as exemplified by five mutants with LoF for β -
141 arr2 recruitment combined with GoF for Ca^{2+} mobilization (p.E408G, p.W417G), for cAMP
142 production (p.I357F) or for both pathways (p.Y291C, p.A316T) (Extended Data Fig. 6d,g,f, Fig.
143 2g).

144 We next performed an unbiased cluster analysis of those mutants for which signaling data were
145 obtained for at least one pathway (56 variants) (Fig. 3). Non-negative matrix factorization (nnmf)
146 and k-means were used to unbiasedly group the variants. To have a unique measure representing
147 the signaling signatures of each variant, we defined the “phenotype score” as the positive-sum
148 average of 12 signaling parameters. The mutants with different signaling profiles fitted best into
149 three distinct clusters (Fig. 3a). Mutants in the first cluster (red, 13 variants) are characterized by
150 complete loss of β -arr2 response and drastically reduced potency of the cAMP response. They
151 also lost mid to high range of efficacy in ERK1/2. In the second cluster (blue, seven variants), β -
152 arr2 responses are detectable, but with drastic losses in E_{\max} and τ/K_a . They also show reduced
153 ERK1/2 efficacy, while increased ERK1/2 potency. Signaling impairments varied in Cluster 3
154 (black, 36 variants) with the variants with the lowest phenotypic scores belonging to this group
155 (Fig 3a,b). The overlay of the different members of each cluster is shown in Fig 3c.

156 We then compared the experimentally obtained phenotypic score for those mutations located in
157 the transmembrane region with six different scoring algorithms including EA, REVEL, CADD,
158 SIFT, PolyPhen2, and MutationAssessor (Extended Data Fig. 8). CADD and EA scores showed
159 the best R squares (0.46 and 0.42). The EA score showed the steepest slope (x-
160 coefficient=0.0101), meaning the best discriminatory information, and showed also the lowest
161 number of false positives (mutants with high predicted score (>80) but low phenotypic score)
162 confirming the high value of the EA score in predicting the effect of variants on receptor fitness
163 (Fig. 3d).

164 Among the *GLPIR* variants that were functionally analyzed *in vitro*, 35 variants were present in
165 the 200K exome data of the UK Biobank (Supplementary Table 1). We could therefore assess
166 the association between these *GLPIR* variants and various metabolic traits in UK Biobank. In
167 the carriers, each *GLPIR* variant was heterozygous. Using the mixed-effects score test (MiST)
168 method adjusted for relevant covariates, the burden of rare, loss-of-function *GLPIR* variants
169 impairing cell surface expression was significantly associated with increased glycated
170 hemoglobin A1c (Hb1Ac) ($P = 6.9 \times 10^{-4}$ with an effect [β] of 0.95 ± 0.28), increased body mass
171 index (BMI) ($P = 2.6 \times 10^{-3}$ with a β of 0.032 ± 0.011) and increased diastolic blood pressure ($P =$
172 0.044 with a β of 1.3 ± 0.62 (Fig. 3e and Extended Data Fig. 9). These associations were stronger
173 when rare, null (*i.e.* nonsense, frameshift, canonical ± 1 or 2 splice sites, start lost) variants in
174 *GLPIR* that were detected in the 200K exome data of the UK Biobank (Supplementary Table 4)
175 were also included in the burden of *GLPIR* variants ($P = 2.8 \times 10^{-4}$ with a β of 0.98 ± 0.27 , $P =$
176 8.7×10^{-4} with a β of 0.034 ± 0.010 and $P = 0.023$ with a β of 1.4 ± 0.60 , respectively) (Fig. 3e and
177 Extended Data Fig. 9). Furthermore, the burden of rare, null *GLPIR* variants along with all rare
178 *GLPIR* variants impairing Ca^{2+} mobilization, β -arr2 recruitment, cAMP pathway and/or cell
179 surface expression strongly increased both HbA1c ($P = 2.7 \times 10^{-4}$ with a β of 0.98 ± 0.27) and BMI
180 levels ($P = 9.9 \times 10^{-4}$ with a β of 0.033 ± 0.010) (Fig. 3e and Extended Data Fig. 9). These
181 associations were even stronger when LoF variants of β -arr2 recruitment were excluded ($P =$
182 1.3×10^{-4} with a β of 1.2 ± 0.30 and $P = 7.2 \times 10^{-4}$ with a β of 0.038 ± 0.011 , respectively) (Fig. 3e
183 and Extended Data Fig. 9). This result suggested that defective β -arr2 recruitment is deleterious
184 for glucose homeostasis and adiposity. **Of note, we did not find any significant associations**
185 **between rare deleterious *GLPIR* variants with EA score ≥ 60 and metabolic traits (Extended Data**
186 **Fig. 9), highlighting the importance of *in vitro* analyses as we show here and in previous**
187 **functional genetics-based studies,^{13, 14, 15} although the number of carriers was lower.** Collectively,
188 these results indicate that impaired *GLPIR* cell surface expression is a risk factor for increased

189 HbA1c, BMI and diastolic blood pressure levels. Impaired β -arr2 recruitment seems to have
190 rather a beneficial effect on these phenotypes, most likely by limiting GLP1R trafficking¹⁶.

191 We then measured incretin promoted glucose-stimulated insulin secretion (GSIS) in INS-1 823/3
192 (*Glp1r* KO) cells. Expression of WT GLP1R restored a functional response by Ex-4 (pEC₅₀ of
193 10.35 ± 0.28 ; $n=4$) and semaglutide (a clinically used GLP1R agonist¹⁷) (pEC₅₀ of 11.20 ± 0.38 ;
194 $n=4$) (Fig. 4a,b and Extended Data Fig. 10a,b). As expected, expression of mutants with LoF on
195 all pathways and severely impaired cell surface expression (*i.e.* p.H180Y, p.N320Y, p.G361R
196 and p.I400R) did not restore an Ex-4 response despite successful expression, even though lower
197 than for WT receptor (Fig. 4c,d, see also Fig. 2b). Expression of mutants in the categories
198 ‘Severely surface exp defective’ and ‘All pathways defective’ but with some residual activity on
199 the cAMP pathway (p.H173P, p.R310Q, p.R380C) did not elicit a response at a low Ex-4
200 concentration, considered as saturating for WT GLP1R (0.1 nM), and most likely not at
201 physiological GLP-1 concentraton. However, the same variants were fully responsive at 100 nM
202 Ex-4 (Fig. 4b, Fig. 4e-g). Similar rescue was observed for p.H173P with 100 nM semaglutide
203 (Fig. 4h). Positive allosteric modulators (PAM) are another potential way to improve the
204 defective response of LoF mutants to orthosteric ligands⁴. Co-stimulation of the p.R380C mutant
205 with 0.1 nM Ex-4 and the GLP1R PAM Compound 2 (10 μ M)^{18, 19, 20} restored a response similar
206 to the incubation with 100 nM Ex-4 alone (Fig. 4i). Compound 2 alone did not have a significant
207 effect on the p.R380C mutant (Fig. 4i). A similar pattern was observed for BETP (10 μ M),
208 another GLP1R PAM, which was also effective on its own revealing its agonistic activity in
209 addition to its allosteric activity (Fig. 4j). Compound 2 and BETP similarly potentiated the
210 response of semaglutide at low concentrations (Fig. 4k,l). Mutants with defective β -arr2
211 recruitment showed WT-like GSIS (Extended Data Fig. 10c-f) indicating that defects in this
212 pathway do not inhibit GSIS. GoF mutants, either of the cAMP pathway alone (p.S261A) or in
213 combination with the Ca²⁺ pathway (p.Y291C, p.A316T) showed GSIS similar to WT GLP1R

214 and endogenous GIP receptors (Extended Data Fig. 4g-i) indicating that the improved signaling
215 had no notable consequences on GSIS in our experimental settings.

216 Taken together, in this study we discovered an unexpected high diversity and impact in terms of
217 functional properties in 56 out of 60 rare *GLP1R* mutants. Our results identify defective cell
218 surface expression and cAMP pathway activation as major determinants of *GLP1R* mutants for
219 defective insulin secretion. This defect can be recovered by two pharmacological paradigms
220 (higher agonist concentrations or a combination of low agonist concentration and allosteric
221 modulators) for some mutants. Carriers of these LoF *GLP1R* variants might thus not only benefit
222 from the latest generations of *GLP1R* agonists including unimolecular *GLP1R*/*GIPR* dual
223 agonists,²¹ but also from recently developed *GLP1R* positive allosteric modulators^{22, 23}. LoF
224 *GLP1R* variants were associated with impaired glucose homeostasis and increased adiposity.
225 Exclusion of LoF mutants for β -arr2 recruitment reinforced this association. This observation
226 supports the concept that β -arr-dependent internalization limits the action of *GLP1R* activation
227 on insulin secretion and suggests that carriers of LoF variants not associated with β -arr could
228 benefit from Gs-biased ligands²⁴.

229 This study has some limitations as we did not further explore the fact that rare *GLP1R* variants
230 are heterozygous and may either impact the phenotype through haplo-insufficiency or have a
231 dominant negative effect on the signalling by the co-expressed WT receptor. Aspects that should
232 be addressed in future studies are the demonstration that PAMs can improve the actions of
233 *GLP1R* agonists in *GLP1R* variant carriers, the impact of mutants on *GLP1R* signaling from
234 intracellular locations, on the recruitment of β -arr1, known to be also involved in insulin secretion
235 and β -cell apoptosis^{25, 26}, and on physiological functions of *GLP1R* other than insulin secretion,
236 such as β -cell proliferation or inhibition of food intake¹.

237

238 **ACKNOWLEDGMENTS**

239 We thank Dr. J Naylor (Cambridge, UK) for kindly providing INS-1 832/3 (*GLP1R* KO) cells
240 and Dr. Mark Scott for giving advice for the selection of β arr-1/ β arr-2 selective siRNA
241 sequences. This work was supported by the Fondation de la Recherche Médicale
242 (jfliu@mail.hust.edu.cn), Agence Nationale de la Recherche (ANR-2011-BSV1-012-01
243 “MLT2D”, ANR-2011-META “MELA-BETES, ANR-21-CE18-0023 “alloGLP1R”), Institut
244 National de la Santé et de la Recherche Médicale (INSERM), Centre National de la Recherche
245 Scientifique (CNRS) and the “Who am I?” laboratory of excellence No.ANR-11-LABX-0071
246 funded by the French Government through its “Investments for the Future” program operated by
247 The French National Research Agency under grant No.ANR-11-IDEX-0005-01. This work was
248 supported by grants from the Ministry of Science and Technology (grant number
249 2018YFA0507003 and 2021ZD0203302 to J. L.), the National Natural Science Foundation of
250 China (NSFC) (grant numbers 81720108031, 81872945 and 31721002 to J. L.). This research
251 has been conducted using the UK Biobank Application #67575. This study was further funded
252 by the French National Research Agency (ANR-10-LABX-46 [European Genomics Institute for
253 Diabetes]), the French National Research Agency (ANR-10-EQPX-07-01 [LIGAN-PM]), the
254 European Research Council (ERC GEPIDIAB – 294785; ERC Reg-Seq – 715575), “France
255 Génomique” consortium (ANR-10-INBS-009) and the National Center for Precision Diabetic
256 Medicine – PreciDIAB, which is jointly supported by the French National Agency for Research
257 (ANR-18-IBHU-0001), by the European Union (FEDER), by the Hauts-de-France Regional
258 Council and by the European Metropolis of Lille (MEL). O.L. gratefully acknowledges support
259 from NIH GM066099. W.G. was supported by a doctoral fellowship from the Chinese
260 Scholarship Council (China).

261

262 **AUTHOR CONTRIBUTIONS**

263 W.G., L.L., R.S., A.B., J.L., and R.J. conceived and designed experiments. Z.F., and G.H. made
264 constructions of variant plasmids and L.H. the non-tagged WT GLP1R plasmid. W.G., L.L.,
265 F.G., E.C., M.O., A.H. performed biochemical experiments. E.H. and O.L. did the clustering
266 analysis. A.P. performed variant impact score analyses. A.B. and P.F. conceived and designed
267 the next-generation sequencing study. A.B., M.D. and M.B. performed the genetic analyses.
268 G.C., M.M., A.B., P.F. and B.B. contributed DNA samples from patients. W.G., L.L., A.B., O.L.,
269 J.D. and R.J. analyzed data. A.B., P.F., J.L., RJ obtained the funding. W.G., A.B., and R.J. wrote
270 the manuscript that was edited and/or approved by all authors.

271

272 **DECLARATION OF INTERESTS**

273 The authors declare no competing interes

274 **FIGURES AND LEGENDS**

275

276 **Figure 1. Selection Process of *GLP1R* Variants and Expression of WT and Mutant GLP1R**
277 **in Cell Models. a,** Selection of 34 rare non-synonymous variants in *GLP1R* (NM_002062.5)
278 from ExAC browser and 25 rare and one frequent *GLP1R* variants from the RaDiO study¹⁰. EA,
279 evolutionary action algorithm; TM, transmembrane domain; ICD, intracellular domain. **b,**
280 Location of the 60 *GLP1R* variants. Mutant positions are labeled in red. The borders of the
281 membrane domain are delineated by the blue box. C-ter, carboxyl-terminal domain; e1 to e3,
282 extracellular loops 1 to 3; i1 to i3, intracellular loops 1 to 3; N-ter, amino-terminal domain. LoF,
283 loss-of-function; T2D, type 2 diabetes. **c,d,** Surface (Sur) and total (To) expression in HEK293T
284 and INS-1 823/3 (*Glp1r* KO) cells was determined by ELISA. **(c)** Expression of WT and mutant
285 GLP1R in HEK293T cells. Cell surface expression is shown at X-axis, total receptor expression
286 as color gradient and the Sur/To ratio as size of the bubble. Statistical significance of differences
287 (compared with WT GLP1R) was determined by one-way analysis of variance and Dunnett's
288 post-test. Sur: * $P < 0.05$, ** $P < 0.001$, *** $P < 0.0001$; Ratio: # $P < 0.05$, ## $P < 0.001$, ### $P <$
289 0.0001 ; Tot: (a) $P < 0.05$, (b) $P < 0.001$, (c) $P < 0.0001$. **(d)** Comparison of cell surface expression
290 of mutants in HEK293T and INS-1 823/3 (*Glp1r* KO) cells. Statistical significance of differences
291 between two cell types was determined by two-way analysis of variance and Sidak's multiple
292 comparisons test * $P < 0.05$, ** $P < 0.01$, *** $P < 0.0001$. 3-5 technical replicates of 3-13
293 independent biological replicates for each mutant; each mutant expressed as % WT. See also
294 Extended Data Fig. 2 and table S2 for complete data sets.

295

296 **Figure 2. Functional Profiling of GLP1R Mutants Define Eight Categories. a-g,** Ex-4
297 concentration-response curves of cAMP production, Ca²⁺ mobilization, ERK activation, and
298 β -arr2 recruitment and radial graphs of one representative GLP1R mutant of each category.
299 Mutant GLP1R (solid lines with filled circles) and WT GLP1R (dotted lines with open
300 circles) were monitored in parallel in each experiment. For radial graphs, data were
301 normalized to WT GLP1R (set as zero), values of mutants ranged from -1 to +1, where 0 to
302 +1 represent enhanced properties, and 0 to -1 represents impaired properties. All values are
303 means \pm SEM of 2-3 technical replicates of 3-8 independent biological replicates for each
304 mutant. Exp, expression; Δ , $\Delta\log(\tau/K_A)$; Ex-4, Exendin-4. See also Extended Data Fig. 4 to
305 Extended Data Fig. 7 and tables S2 and S3 for complete data sets for the agonist-mediated
306 signaling activity of GLP1R mutants.

307

308 **Figure 3. 56 Mutants Clustered into Three Groups are Correlated to the Level of**
309 **Phenotypic Pb. a,** Non-Negative Matrix Factorization (NMF) and K-means analysis
310 clustered 56 mutants into 3 groups as shown in three dendrograms (red, blue, and black). The
311 normalized difference values from phenotypic assays are represented in each radial plot and
312 color-coded blue (Gain-of-Function, GoF) to red (Loss-of-Function, LoF). Phenotype scores
313 were set from -1 to +1. WT GLP1R was set as zero, values of mutants ranging from 0 to +1
314 represent enhanced properties, and from 0 to -1 impaired properties. **b,** The box plot shows
315 the distribution of the mutants into three clusters based on their phenotype score defined in
316 the 'Methods' section. **c,** Superimposed radial graphs of mutants belonging to the same
317 cluster. Cluster 1 is characterized by a complete loss of β -arr2 response and also drastically
318 reduced potency of the cAMP response. They also lost mid to high ERK efficacy. Cluster 2
319 shows detectable β -arr2 function but drastic losses in Emax and $\log(\tau/K_A)$. These mutants
320 also have reduced ERK efficacy but increased ERK potency. Member of Cluster 3 shows

321 lower phenotype scores than those of the other two clusters. **d**, The predictive evolutionary
322 Action (EA) score of GLP1R mutants in the TM domain is correlated with the experimentally
323 determined Phenotypic score of these mutants. $R^2=0.41$ for the linear correlation ($P <$
324 0.0001). **The TM domain was selected because of its highest predictive value for GPCRs** ²⁷,
325 Pb, Perturbatio. **e**, Association between rare GLP1R variants and metabolic traits in the UK
326 Biobank. β -arr2, beta arrestin 2; BMI, body mass index; DBP, diastolic blood pressure;
327 HbA1c, glycated hemoglobin A1C; HDL, high-density lipoprotein; LDL, low-density
328 lipoprotein; SBP, systolic blood pressure; SE, standard error.

329

330 **Figure 4. Rescue of Insulin Secretion of GLP1R Mutants Expressed in INS-1 823/3**

331 (***Glp1r* KO**) cells. INS-1 823/3 (*Glp1r* KO) pancreatic β -cell line deleted of its *Glp1r* gene
332 was used to examine the capacity of GLP1R mutants to promote glucose-stimulated insulin
333 secretion. **a**, Ex-4 (100 nM) and GIP (100 nM) response in mock-transfected cells. **b**, Ex-4
334 concentration-response curve in cells expressing GLP1R WT. **c**, Total expression of mutants
335 determined by ELISA. **d-g**, Ex-4 response in cells expressing mutants with (**d,e**) severely
336 defective cell surface expression or (**f,g**) severely defective cAMP pathway (2 logs right
337 shifted EC_{50}). **h**, **Semaglutide response in cells expressing WT GLP1R, p.H173P, p.R310Q or**
338 **p.R380C mutants**. **i,j**, Ex-4 response in the presence of Compound 2 or BETP in cells
339 expressing the p.R380C mutant. **k,l**, **Semaglutide response in the presence of Compound 2 or**
340 **BETP in cells expressing the p.R380C mutant**. Responses are normalized to glucose-induced
341 insulin secretion in the absence of Ex-4. All values are means \pm SEM of at least three
342 independent experiments. Statistical significance of differences (compared with control) was
343 determined by one-way analysis of variance and Dunnett's post-test $*P < 0.05$, $**P < 0.01$,
344 $***P < 0.0001$. Statistical significance of differences (compared with 0.1 nM treatment of
345 GLP1R mutant) was determined by one-way analysis of variance and Dunnett's post-test $\#P$

346 < 0.05 , $###P < 0.0001$. Ex-4, Exendin-4; G-ctrl, glucose control; Comp 2, Compound 2;

347 Sema, Semaglutide.

348

349 **METHODS**

350 *Studies in cellular models*

351 HEK293T cells (RRID: CVCL 0063) were cultured in Dulbecco's modified Eagle's medium
352 (DMEM, GIBCO, 10566) consisting of 10% fetal bovine serum (FBS), 100 U/ml penicillin, and
353 0.1 mg/ml streptomycin. INS-1 832/3 cells lacking endogenous Glp1r after deletion by CRISPR-
354 Cas9¹¹, a gift from Dr Jacqueline Naylor, were cultured in RPMI-1640 medium (Invitrogen),
355 supplemented with 10% FBS, 100 U/ml penicillin, 0.1 mg/ml streptomycin, 1 mM sodium
356 pyruvate, 10 mM HEPES and 50 μM 2-mercaptoethanol. Cells were incubated in a humidified
357 air incubator containing 5% CO₂ at 37°C.

358 *GLP1R gene sequencing*

359 Participants included in the RaDiO study were previously described (Nat Med. 2019
360 Nov;25(11):1733-1738. // Nat Metab. 2020 Oct;2(10):1126-1134.). DNA sequencing of *GLP1R*
361 (NM_002062.5) was performed by next-generation sequencing as previously described (Nat
362 Med. 2019 Nov;25(11):1733-1738. // Nat Metab. 2020 Oct;2(10):1126-1134.). Briefly,
363 NimbleGen SeqCap EZ Choice XL target enrichment (Roche, Pleasanton, USA) was performed
364 according to the manufacturer's protocol for next-generation sequencing on the HiSeq 4000
365 system (Illumina, San Diego, USA), using a paired-end 2×150 bp protocol. The demultiplexing
366 of sequence data was performed using bcl2fastq Conversion Software (Illumina; v2.17).
367 Sequence reads were then mapped to the human genome (hg19/GRCh37) using Burrows-
368 Wheeler Aligner (v0.7.13). The variant calling was performed using Genome Analysis ToolKit
369 (GATK; v3.3). Only variants with a coverage higher than 8 reads were kept for further analyses.
370 The annotation of variants was performed using the Ensembl Perl Application Program Interfaces
371 (v75) and custom Perl scripts to include data from both dbSNP (version 135) and dbNSFP (v3.0)
372 databases. All coding variants had a QUAL score higher than 50. Furthermore, no variant had

373 more than 5% missing genotype (with a coverage below 8 reads or a QUAL score below 50)
374 across the participants.

375 In UK Biobank (Application #67575), we analyzed up to 187,743 samples, with available exome
376 sequencing data and clinical data. More specifically, we used exome data from pVCF format
377 (field #23156). Only variants with a coverage higher than 10 reads and quality GQ score higher
378 than 20 were kept for further analyses. Annotation of variants in *GLP1R* (NM_002062.5) was
379 done using the Ensembl Variant Effect Predictor (VEP) tool version 103 (RefSeq). Subsequently,
380 the analysis was focused on loss-of-function variants. No loss-of-function variant had more than
381 5% missing genotype (*i.e.* with a coverage below 10 reads or a GQ score below 20) across the
382 participants.

383 ***Selection of GLP1R coding variants for functional in vitro analysis***

384 In 2016, the ExAC browser (previous version of Genome Aggregation Database [GnomAD])
385 included 132 nonsynonymous variants in *GLP1R* (NM_002062.5), including five common
386 variants with a MAF higher than 1% (Fig. 1 and table S1). To predict the functional impact of
387 these variants in silico, we determined their evolutionary action (EA) score ⁷ (Extended Data Fig.
388 1). The EA has been shown to usefully predict the functional impact of mutations in genes
389 encoding GPCRs ^{14, 27}. It takes into account the relative importance of each residue position
390 estimated with the evolutionary trace method based on phylogenetic divergences ⁸, combined
391 with the likelihood to observe a given amino acid substitution at that position in receptor
392 homologs across evolution ⁷. We selected 44 missense *GLP1R* variants predicted to be of
393 moderate to high impact based on their EA scores. Available literature data on the functional
394 consequences of alanine mutations at 11 positions among the positions of the 132 variants guided
395 us further in the selection of the most impactful variants (Fig. 1). To further narrow down the
396 number of variants we focused on mutations located in the TM and intracellular domains, both
397 known to be important for receptor activation and signal transduction. At the end this selection

398 process, we focused on 34 rare variants with high predicted functional impact (Fig. 1, Extended
399 Data Fig. 1a and table S1). In parallel, we performed sequencing of *GLP1R* exons
400 (NM_002062.5) in 8,672 participants from the RaDiO study¹⁰. We identified 46 nonsynonymous
401 variants of which we selected 25 rare variants and a common one encoding p.A316T because of
402 their high predicted functional impact (Fig. 1, Extended Data Fig. 1b and table S1). In total, 60
403 *GLP1R* variants were selected for *in vitro* functional analyses (see Fig. 1b for positions in the
404 receptor).

405 ***Receptor mutagenesis and constructs***

406 GLP1R cDNA construct containing an N-terminal SNAP tag fused to a FLAG tag were obtained
407 from Cisbio Bioassays (Codolet, France). GLP1R mutants were generated by site-directed
408 mutagenesis using QuikChange Lightning Site-Directed Mutagenesis Kit (Agilent Technologies,
409 210518) according to the manufacturer's protocols. The non-tagged GLP1R was generated by
410 replacing the SNAP-flag cassette and by an oligonucleotide reconstituting the N-terminal
411 methionine residue. All constructs were verified with Eurofins sequencing.

412 ***Transfection of plasmids and siRNA***

413 HEK293T cells were transiently transfected with plasmid DNA by the reagent JetPEI (101-10N,
414 Polyplus, New York, NY, USA) and transfected with siRNA using INTERFERin® (101000028,
415 Polyplus, Illkirch, FRANCE) according to the manufacturer's instructions. INS-1 832/3 (*Glp1r*
416 KO) cells were transiently transfected with Lipofectamine® LTX & Plus Reagent (15338-100,
417 Invitrogen) according to the manufacturer's instructions. Generally, cells were 50–70% confluent
418 at the time of transfection. At least forty-eight hours after transfection, both HEK293T and INS-
419 1 832/3 (*Glp1r* KO) cells were experimentally manipulated for all the ELISA and signaling
420 assays. The double-stranded 5'-ACCUGCGCCUCCGCUAUG-3' siRNA sequence
421 (Eurogentec) was used to simultaneously target both β arr-1 and β arr-2, as described previously
422 ²⁸.

423 ***Cell surface and total receptor expression***

424 HEK293T and INS-1 832/3 (*Glp1r* KO) cells were transfected with GLP1R or mutant receptor
425 cDNA construct containing an N-terminal SNAP tag fused to a FLAG tag. After 24h, the cells
426 were seeded into 96-well white Optiplates (6005680, Perkin Elmer) and cultured overnight at
427 37°C in 5% CO₂. To measure the surface expression, the ELISA cells were washed with 1x PBS
428 and fixed with 2% paraformaldehyde (PFA) at room temperature for 10 min. For total receptor
429 measurement, cells washed with 1x PBS and fixed with methanol/acetone (1: 1) at room
430 temperature for 1 min and then additionally treated with 0.2% Triton X-100 at room temperature
431 for 10 min. The cells are blocked over 1 hour by 3% BSA for surface expression and 3% BSA
432 containing 0.2% Triton X-100 for total expression. Receptor expression was then measured using
433 a rabbit anti-flag antibody (F7425, Sigma-Aldrich) and a horseradish peroxidase-conjugated
434 rabbit immunoglobulin G (IgG) secondary antibody (Cell signaling, 7074S). Luminata™ Forte
435 ELISA HRP substrate (ELLUF0100, Merck Millipore) was used for the reaction to generate
436 luminescence. Luminescence was read with a Tecan Infinite M500 microplate reader (Tecan
437 Group, Ltd., Männedorf, Switzerland). No interference of the **N-terminal SNAP-flag-tag was**
438 **observed as similar results were observed with the non-tagged and the SNAP-flag-tagged WT**
439 **GLP1R in INS-1 823/3 (*Glp1r* KO) and HEK293T cells (Extended Data Fig. 3g-j).**

440 For internalization assays cells are incubated with 100 nM exendin-4 (Bachem, Weil am Rhein,
441 Germany) at 37°C in 5% CO₂ for the indicated times. The amount of surface and total receptors
442 were then determined by ELISA.

443 ***LUXendin Flow cytometry***

444 **12 week-old C57/BL6 (Janvier, France) male mouse islet isolation was performed as described**
445 **previously²⁹. Islets were cultured in RPMI 1640 (#61870-010, Thermo Fisher Scientific)**
446 **containing 10% fetal calf serum (FCS CVFVSF00-01, Eurobio, Les Ulis, France) and**
447 **penicillin/streptomycin (#15140122, ThermoFisher Scientific) at 37°C, 5% CO₂. Islets were**

448 incubated with 100 nM of LUXendin¹² (Celtarys CELT111), or with 10 μ M Exendin-4 (Bachem,
449 Weil am Rhein, Germany) for 1h. Islets were then dissociated in single cell suspensions using
450 Accutase (#07922, Stemcell technologies, Vancouver, Canada). GLP1R or Mock transfected
451 INS-1 832/3 (*Glp1r* KO) and HEK293T were incubated with 100 nM of LUXendin for 1h and
452 detached with trypsin. Cell sorting was carried out using a FACSAria III (BD Bioscience). Data
453 were analyzed using FlowJo™ Software (RRID:SCR_008520, BD Life Sciences). LUXendin-
454 positive cells were sorted in several sequential steps as described in Supplementary Figure 1. Data
455 were normalized by subtracting background staining (Mock transfected INS-1 832/3 (*Glp1r*
456 KO) and HEK293T or Exendin-4 excess (GLP1R+ beta-cells) and are expressed as Mean
457 Fluorescent Intensity (MFI) per cell.

458

459 ***cAMP accumulation measurement***

460 Ligands-mediated cAMP accumulation assays were performed using the cAMP Gi kit
461 (62AM9PEB, Cisbio Bioassays) as previously described³⁰. Cells transiently expressed GLP1R
462 WT or mutants. Forty-eight hours post-transfection, cells were suspended in stimulation buffer
463 from kit and distributed to a 384-well white ProxiPlate (6008280, Perkin Elmer) at a density of
464 7500 cells per well. Increasing concentration of ligands was added to cell suspension. After
465 30min stimulation, cAMP d2 antibody and cAMP Eu-cryptate reagent were added. After one
466 hour of stimulation, cAMP measurements were performed in triplicates and were read in Tecan
467 Infinite M500 microplate (Tecan Group, Ltd., Männedorf, Switzerland).

468 ***ERK activation measurement***

469 Intracellular phospho-ERK1/2 was measured using the AlphaLISA Surefire pERK kit as
470 described previously³¹ (ALSU-PERK-A500, PerkinElmer, Waltham, MA). HEK293T cells
471 transiently expressed GLP1R WT or one of the 60 GLP1R mutants. The cells are starved
472 overnight prior to stimulation. An increasing concentration of ligands diluted in DMEM

473 (Invitrogen) free FBS, was added at 37°C for the indicated times to generate full concentration-
474 response curves. Cellular lysates were generated by adding the lysis buffer. Four µl cellular
475 lysates were transferred to a 384-well white ProxiPlate (6008280, Perkin Elmer). After the
476 reaction mixture was added and the signal was detected using the Tecan Infinite M1000 PRO
477 microplate reader (Tecan Group, Ltd., Männedorf, Switzerland) with excitation at 680nm (α -
478 laser) and emission at 520-620nm.

479 Exendin-4 induced ERK1/2 phosphorylation kinetics was determined over 1 h. At 5min, the
480 exendin-4-mediated pERK1/2 was maximal for HEK293T cells. Accordingly, pERK1/2 dose-
481 response experiments were performed at 5 min. At 5 min the Gs/cAMP/PKA pathway was the
482 predominant input pathway (Extended Data Fig. 3k-n).

483

484 ***Intracellular calcium mobilization measurement***

485 Intracellular Ca²⁺ mobilization detected in HEK293T cells was performed as previously
486 described. Briefly, cells were pre-incubated with the Ca²⁺-sensitive Fluo-4 AM (Thermo Fisher
487 Scientific) in 37°C incubator for 1 h before measuring in the multi-mode microplate reader
488 (FlexStation 3, Molecular Devices). The fluorescence signals (excitation at 485 nm and emission
489 at 525 nm) were then measured for 60 s. After the first 20 s, compounds were added automatically
490 into the plate to treat the cells. The Ca²⁺ response was given as the agonist-induced fluorescence
491 increase (maximum signal after agonist addition subtracts the mean value of the first 20 s). The
492 dependence of the Ca response on Gq/11 proteins was addressed by preincubating cells for 30
493 min with the Gq/11 protein specific YM-254890 inhibitor in the presence of Ex-4 (100 nM)
494 (Extended Data Fig. 3o).

495 ***β -arr2 recruitment (BRET) measurement***

496 β -arr2 recruitment by GLP1R at the cell surface was assessed by measuring BRET between
497 RlucII- β -arr2 and rGFP-CAAX (prenylation CAAX box of KRas) upon treatment of HEK 293T

498 cells cotransfected with GLP1R. Transfected cells were plated in 96-well white Optiplates
499 (6005680, Perkin Elmer). Forty-eight hours after transfection, cells were washed with
500 Dulbecco's phosphate-buffered saline, and then Tyrode's buffer was added. After 5 min
501 incubation with Deep blue C Coelenterazine (2.5 μ M, NanoLight Technology), the cells were
502 incubated for 5 more minutes with exendin-4 at 37°C. Then, luminescence and fluorescence were
503 measured simultaneously using plates and were read on the Mithras LB 940 with 480 ± 10 nm
504 (Rluc) and 540 ± 20 nm (YFP) emission filters and BRET ratios were calculated.

505 ***Insulin secretion measurement***

506 INS-1 832/3 (*Glp1r* KO) cells were seeded into 24-well plates coated with poly-L-lysine
507 hydrobromide (P6282, Sigma-Aldrich). GLP1R or one of the 60 GLP1R mutants were
508 transfected one day after. The cultured medium was changed by fresh cultured medium 24 h prior
509 to glucose-dependent insulin secretion. On the day of the experiment, the cells were washed three
510 times by low-glucose (2.8 mM) Krebs Ringer buffer (2.6 mM CaCl₂, 98.5 mM NaCl, 4 mM KCl,
511 1.2 mM KH₂PO₄, 1.2 mM MgSO₄, 20 mM HEPES, 25.9 mM NaHCO₃, 0.2% BSA, pH 7.4)
512 and incubated for 1 h at 37°C in low-glucose (2.8 mM) Krebs Ringer buffer. The supernatant
513 was removed, and cells were incubated for 1 h at 37°C in high-(8.3 mM) glucose Krebs Ringer
514 buffer \pm exendin-4 or GIP or semaglutide ¹¹. The supernatant was collected and insulin
515 concentration was measured in 10 μ L using the Insulin Ultra Sensitive assay (62IN2PEG, Cisbio
516 Bioassays). According to the manufacturer's instructions, supernatant, insulin Eu³⁺ Cryptate
517 antibody and insulin XL665 antibody were distributed in a 384-well microplate (6007290, Perkin
518 Elmer). After 24 hours incubation, the signal was read in Tecan Infinite M500 microplate (Tecan
519 Group, Ltd., Männedorf, Switzerland).

520 ***TR-FRET-based ligand competition binding measurement***

521 The affinity of GLP1R WT and GLP1R mutants for exendin-4 were determined by TR-FRET-
522 based ligand competitive binding assay. Forty-eight hours post-transfection, HEK293T cells

523 expressing SNAP-GLP1R WT or mutants were immediately placed on the ice to avoid the rapid
524 receptor internalization. After washes, the cells were incubated with substrate (100 nM)
525 conjugated to the long-lived fluorophore Terbium cryptate (Tb; Lumi4-Tb, SSNPTBX, Cisbio
526 Bioassays) in Tag-lite labeling medium (1 h, on ice, LABMED, Cisbio Bioassays). After several
527 washes, cells were dissociated by enzyme-free cell dissociation buffer (C5789; Sigma-Aldrich)
528 and resuspended in Tag-lite buffer. The cells are distributed into a 384-well plate, whose then
529 were used to detect fluorescence signal at 620 nm for verification of the efficiency of fluorescent
530 labeling of SNAP. An increasing concentration of exendin-4 was incubated with cells in the
531 presence or absence of the exendin-4 derivative labeled with a red-emitting HTRF fluorescent
532 probe (L0030RED, Cisbio Bioassays) at final reaction volume of 14 μ L. The incubation last two
533 hours at room temperature and the TR-FRET signal was read in the Tecan Infinite M500
534 microplate reader (Tecan Group, Ltd., Männedorf, Switzerland) following settings: excitation at
535 340 nm (Tb, energy donor), emission at 665 nm (d2, acceptor); and 620 nm (donor); delay of
536 150 μ s; and integration time of 500 μ s. Data is expressed as TR-FRET ratio (acceptor/donor) or
537 normalized as % when indicated (maximal TR-FRET ratio = 100%, non-specific binding = 0%).

538 ***Western blotting***

539 HEK293T cells were seeded in 6-well plates and transiently expressed GLP1R and silenced by
540 using siRNA targeting both β -arr1 and β -arr2 according to the manufacturer's instructions. The
541 cells were then washed with PBS carefully. Lysis buffer composed of 62.5mM Tris/HCl pH 6.8,
542 5% SDS, 10% glycerol, 0.005% bromophenol blue are applied to denature proteins in cells over
543 2 hours. Samples were then sonicated for 5s, three times, and heated for 5 min at 95 °C. Denatured
544 protein samples were resolved in SDS-PAGE and then transferred to nitrocellulose membranes.
545 The immunoblottings were carried out with primary antibodies against the Flag tag (F7425,
546 Sigma-Aldrich) and β -arr1/2 (4674, Cell Signaling Technology). Immunoreactivity was revealed
547 using a secondary antibody coupled to 680 or 800 nm fluorophores (LI-COR Biosciences,

548 Lincoln, NE, USA), and readings were performed with the Odyssey LI-COR infrared fluorescent
549 scanner (LI-COR Biosciences).

550 *NMF/K-mean Clustering Analysis*

551 To characterize the phenotypic effects of the GLP1R mutants, we applied the Non-Negative
552 Matrix Factorization (NMF) and K-means clustering analysis described in ²⁷. Among the 60
553 mutants tested on GLP1R, four mutants (p.H180Y, p.N320Y, p.G361R, and p. I400R) were
554 excluded because their experimental data were undetectable. To initiate the clustering, an input
555 matrix was generated with 56 mutants and 4 different signaling pathways (β -arr2, Ca²⁺, cAMP,
556 and ERK) measured by 3 parameters each (E_{max} , EC_{50} , and $\Delta\log(\tau/K_A)$), which resulted in matrix
557 size of 56 x 12. To establish the robustness of the results, experimental errors were propagated
558 by iteratively sampling values within one standard deviation of the mean of the phenotypic
559 measurement. This generated a background of 300 input matrices that were independently
560 processed by NMF/K-mean clustering. Before applying the clustering algorithm, each
561 phenotypic measurement was normalized against WT:

562
$$\text{Normalized Difference Value}_{ij} = \frac{x_{ij} - WT_j}{x_{ij} + WT_j} + 1 \quad (1),$$

563 where x_{ij} indicates the j phenotypic measurement on mutant i , and WT_j indicates wild type values
564 on the j phenotypic measurement. Therefore, each value ranged from 0 to 2, where 1 indicates
565 an activity similar to WT. NMF was performed in the normalized matrix from
566 sklearn.decomposition package in python to reduce dimensionality [K (basis factor) x H (number
567 of mutants)]. We applied K-means analysis to the result of dimension reduction, using the
568 sklearn.cluster package in python, across K=2 to K=5, where K is basis factor for NMF and the
569 number of clusters for K-means (KNMF=KKmean). For each input matrix, NMF/K-means was
570 iteratively applied 300 times. Thus, the final clustering frequency was determined by averaging
571 90,000 outcomes (300 input matrix times 300 clustering iteration) and converted into Euclidean
572 distance matrix, using the scipy.cluster package in python.

573 ***Evolutionary Action Scores***

574 The Evolutionary Action (EA) of a mutation is computed with an equation ⁷:

575
$$d\phi = \nabla f \cdot d\gamma. \quad (2),$$

576 where f is a fitness function that maps genotypes, γ , to phenotypes, ϕ , so that we may write
577 $f(\gamma) = \phi$. In practice, Eqn 2 can be computed by estimating $d\phi$ as the magnitude of a mutation
578 from evolutionary odds matrices of amino acid substitutions, and estimating ∇f , which as the
579 gradient of the evolutionary function represent the functional sensitivity to mutations at each
580 sequence positions, with the Evolutionary Trace ⁸. The result is the EA, $d\phi$, which varies
581 continuously from 0 (a neutral mutation with no fitness effect) to 100 (a maximally deleterious
582 mutation that causes a functional knockout). EA scores below 30 tend to be harmless, but tend
583 to impact function progressively more above that threshold. The GLP1R mutants EA scores were
584 given from <http://eaction.lichtargelab.org/eaction>. To evaluate EA score prediction with the
585 experimental data, phenotypic score was calculated thus:

586
$$\text{Phenotypic Score}_i = \sum_{j=0}^n |y_{ij}|$$

587
$$y_{ij} = \frac{x_{ij} - \text{WT}_j}{x_{ij} + \text{WT}_j},$$

588 ***Statistical analysis***

589 ***Statistical analyses for genetic association studies.*** In UK Biobank, the rare variants were
590 analyzed as single clusters using the mixed-effects score test (MiST) method (Sun, J., Zheng, Y.
591 & Hsu, L. A unified mixed-effects model for rare-variant association in sequencing studies.
592 *Genet. Epidemiol.* **37**, 334–344 (2013)). MiST provides a score statistic $S(\pi)$ for the mean effect
593 (π) of the cluster, and a score statistic $S(\tau)$ for the heterogeneous effect (τ) of the cluster. Let the
594 equation of the model be: $Y = \alpha X + \pi GZ$, where Y is the trait of interest, X is the matrix of
595 covariates (*i.e.* age, sex, body mass index [BMI], ancestry [*i.e.* PC1 to PC5; field #22009] for

596 assessing diastolic blood pressure, systolic blood pressure, high-density lipoprotein, low-density
597 lipoprotein and age, sex, ancestry for assessing BMI and glycated hemoglobin A1c), G is the
598 matrix of *OPRDI* variants and Z is a vector of ones repeated n times, with n the number of rare
599 *OPRDI* variants, leading to: $\pi GZ = \pi \sum_{i=1}^n G_i$. BMI was log-transformed before analysis. As
600 none of the association studies had significant heterogeneity, we only showed the P -values
601 associated with the mean effect (π) of the cluster. These statistical analyses were performed using
602 R software (v4.0.2).

603 ***The surface and total expression determined by ELISA.*** All values are expressed as means \pm
604 SEM of at least three independent experiments. Statistical significance of differences was
605 determined by one-way analysis of variance and Dunnett's post-test.

606 ***Insulin secretion measurement.*** The agonist-induced response for every GLP1R mutant was
607 normalized to its glucose control (set at 1). The fold ratio is expressed as means \pm SEM of at least
608 three independent experiments and compared to the WT receptor in parallel with the receptor
609 mutant. Statistical significance of differences was determined by one-way analysis of variance
610 and Dunnett's post-test. LogEC₅₀ is defined as the log of the concentration of initiating half of
611 the maximal response was determined by nonlinear regression with a variable Hill slope using
612 GraphPad Prism software (version 7.0).

613 ***TR-FRET-based ligand competition binding measurement.*** LogIC₅₀ is defined as the log of the
614 concentration of red-emitting Ex-4 that results in half-way of decreasing of Ex-4 binding. logIC₅₀
615 was determined by nonlinear regression with a variable Hill slope using GraphPad Prism
616 software (version 7.0). LogIC₅₀ is expressed as means \pm SEM of at least three independent
617 experiments. The data were analyzed by comparing independent fits with a global fit that shares
618 the selected parameter and by two-way analysis of variance and Sidak post-test.

619 ***cAMP accumulation, ERK activation, Ca²⁺ mobilization and β -arr2 recruitment***
620 ***measurement.*** Agonist-induced E_{max} is defined as the maximal response generated by agonists.

621 LogEC₅₀, and agonist-induced E_{max} values were determined by nonlinear regression with a
622 variable Hill slope using GraphPad Prism software (version 7.0).

623 For these assays, the agonist-induced E_{max} value for every GLP1R mutant was normalized as a
624 percentage of the maximal Ex-4 stimulated response of the WT receptor (set at 100) monitored
625 in parallel with the receptor mutant. LogEC₅₀ and agonist-induced E_{max} are expressed as means
626 ± SEM of at least three independent experiments. The data were analyzed by comparing
627 independent fits with a global fit that shares the selected parameter and by two-way analysis of
628 variance and Sidak post-test. The concentration-response curves were fitted to an operational
629 model of agonism designed by Kenakin and Christopoulos^{32, 33} to obtain log(τ/K_A) values for
630 the WT receptor and its mutants. Normally, an agonist is set as a reference agonist, against which
631 within pathway comparisons for the same receptor to other agonists can be made and expressed
632 as Δlog(τ/K_A). Here, withinpathway comparisons were made between GLP1R mutants and the
633 WT receptor. Normalized difference was calculated on values corresponding to agonist-induced
634 E_{max}, and Δlog(τ/K_A) to fit a -1 to +1 scale using the following formula: (mutant – WT)/(mutant
635 + WT). In the case of Δlog(τ/K_A), before normalization, the antilogs were first calculated and
636 then were fitted to the following formula: (mutant – WT)/(mutant + WT). Positive and negative
637 values represent mutations with better or worst responses, respectively than those of the WT
638 receptor. Subsequently, Δlog(τ/K_A) values were expressed as means ± SEM of the indicated
639 number of experiments (n). Statistical analysis for Δlog(τ/K_A) ratios was performed by one-
640 sample t test to examine the mean differences between WT GLP1R and its mutants.

641 All the correlation studies are analyzed by linear regression and define R² using GraphPad Prism
642 software (version 7.0). The statistical significance of differences was determined by linear
643 regression.

644

645 Further information and requests for resources and reagents should be directed to and will be
646 fulfilled by the Lead Contact, Ralf Jockers (ralf.jockers@inserm.fr)

647

648 **REFERENCES**

649

650

651 1. Muller TD, *et al.* Glucagon-like peptide 1 (GLP-1). *Mol Metab* **30**, 72-130 (2019).

652

653 2. Graaf C, *et al.* Glucagon-Like Peptide-1 and Its Class B G Protein-Coupled Receptors:
654 A Long March to Therapeutic Successes. *Pharmacol Rev* **68**, 954-1013 (2016).

655

656 3. Zhang Y, *et al.* Cryo-EM structure of the activated GLP-1 receptor in complex with a G
657 protein. *Nature* **546**, 248-253 (2017).

658

659 4. Koole C, *et al.* Polymorphism and ligand dependent changes in human glucagon-like
660 peptide-1 receptor (GLP-1R) function: allosteric rescue of loss of function mutation.
661 *Mol Pharmacol* **80**, 486-497 (2011).

662

663 5. Koole C, Savage EE, Christopoulos A, Miller LJ, Sexton PM, Wootten D. Minireview:
664 Signal bias, allostherism, and polymorphic variation at the GLP-1R: implications for
665 drug discovery. *Mol Endocrinol* **27**, 1234-1244 (2013).

666

667 6. Liu T, Ji RL, Tao YX. Naturally occurring mutations in G protein-coupled receptors
668 associated with obesity and type 2 diabetes mellitus. *Pharmacol Ther* **234**, 108044
669 (2022).

670

671 7. Katsonis P, Lichtarge O. A formal perturbation equation between genotype and
672 phenotype determines the Evolutionary Action of protein-coding variations on fitness.
673 *Genome Res* **24**, 2050-2058 (2014).

674

675 8. Lichtarge O, Bourne HR, Cohen FE. An evolutionary trace method defines binding
676 surfaces common to protein families. *J Mol Biol* **257**, 342-358 (1996).

677

678 9. Wootten D, *et al.* The Extracellular Surface of the GLP-1 Receptor Is a Molecular
679 Trigger for Biased Agonism. *Cell* **165**, 1632-1643 (2016).

680

681 10. Bonnefond A, *et al.* Pathogenic variants in actionable MODY genes are associated
682 with type 2 diabetes. *Nat Metab* **2**, 1126-1134 (2020).

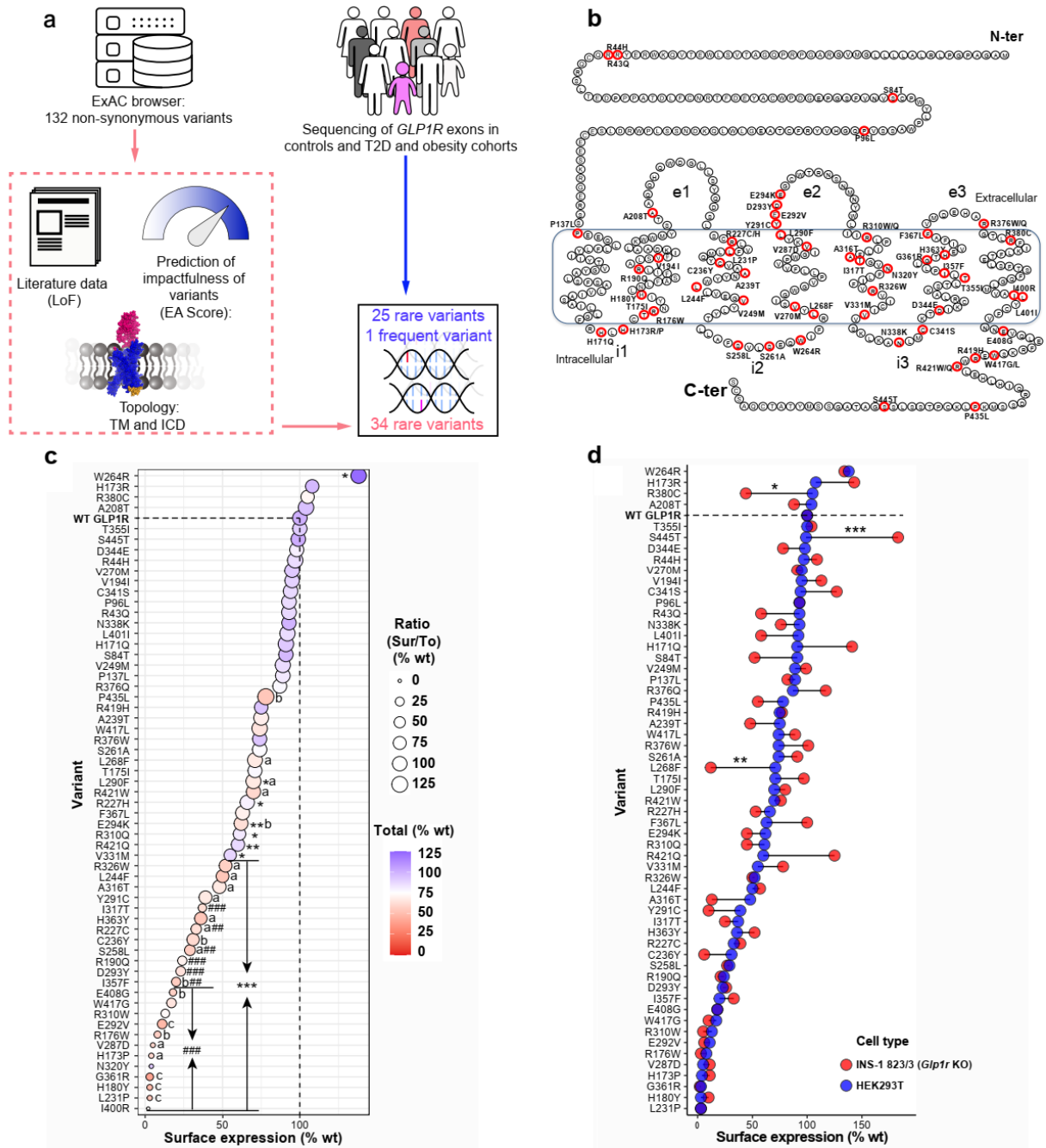
683

-
- 684 11. Naylor J, *et al.* Use of CRISPR/Cas9-engineered INS-1 pancreatic beta cells to define
685 the pharmacology of dual GIPR/GLP-1R agonists. *Biochem J* **473**, 2881-2891 (2016).
- 686
687 12. Ast J, *et al.* Super-resolution microscopy compatible fluorescent probes reveal
688 endogenous glucagon-like peptide-1 receptor distribution and dynamics. *Nat*
689 *Commun* **11**, 467 (2020).
- 690
691 13. Bonnefond A, *et al.* Rare MTNR1B variants impairing melatonin receptor 1B function
692 contribute to type 2 diabetes. *Nat Genet* **44**, 297-301 (2012).
- 693
694 14. Karamitri A, *et al.* Type 2 diabetes-associated variants of the MT(2) melatonin
695 receptor affect distinct modes of signaling. *Sci Signal* **11**, (2018).
- 696
697 15. Folon L, *et al.* Contribution of heterozygous PCSK1 variants to obesity and
698 implications for precision medicine: a case-control study. *Lancet Diabetes Endocrinol*
699 **11**, 182-190 (2023).
- 700
701 16. Jones B, *et al.* Targeting GLP-1 receptor trafficking to improve agonist efficacy. *Nat*
702 *Commun* **9**, 1602 (2018).
- 703
704 17. Kushner RF, *et al.* Semaglutide 2.4 mg for the Treatment of Obesity: Key Elements of
705 the STEP Trials 1 to 5. *Obesity (Silver Spring)* **28**, 1050-1061 (2020).
- 706
707 18. Knudsen LB, *et al.* Small-molecule agonists for the glucagon-like peptide 1 receptor.
708 *Proc Natl Acad Sci U S A* **104**, 937-942 (2007).
- 709
710 19. Koole C, *et al.* Allosteric ligands of the glucagon-like peptide 1 receptor (GLP-1R)
711 differentially modulate endogenous and exogenous peptide responses in a pathway-
712 selective manner: implications for drug screening. *Mol Pharmacol* **78**, 456-465
713 (2010).
- 714
715 20. Wootten D, *et al.* Differential activation and modulation of the glucagon-like peptide-
716 1 receptor by small molecule ligands. *Mol Pharmacol* **83**, 822-834 (2013).
- 717
718 21. Rosenstock J, *et al.* Efficacy and safety of a novel dual GIP and GLP-1 receptor
719 agonist tirzepatide in patients with type 2 diabetes (SURPASS-1): a double-blind,
720 randomised, phase 3 trial. *Lancet* **398**, 143-155 (2021).
- 721
722 22. Malik F, Li Z. Non-peptide agonists and positive allosteric modulators of glucagon-like
723 peptide-1 receptors: Alternative approaches for treatment of Type 2 diabetes. *Br J*
724 *Pharmacol* **179**, 511-525 (2022).

725

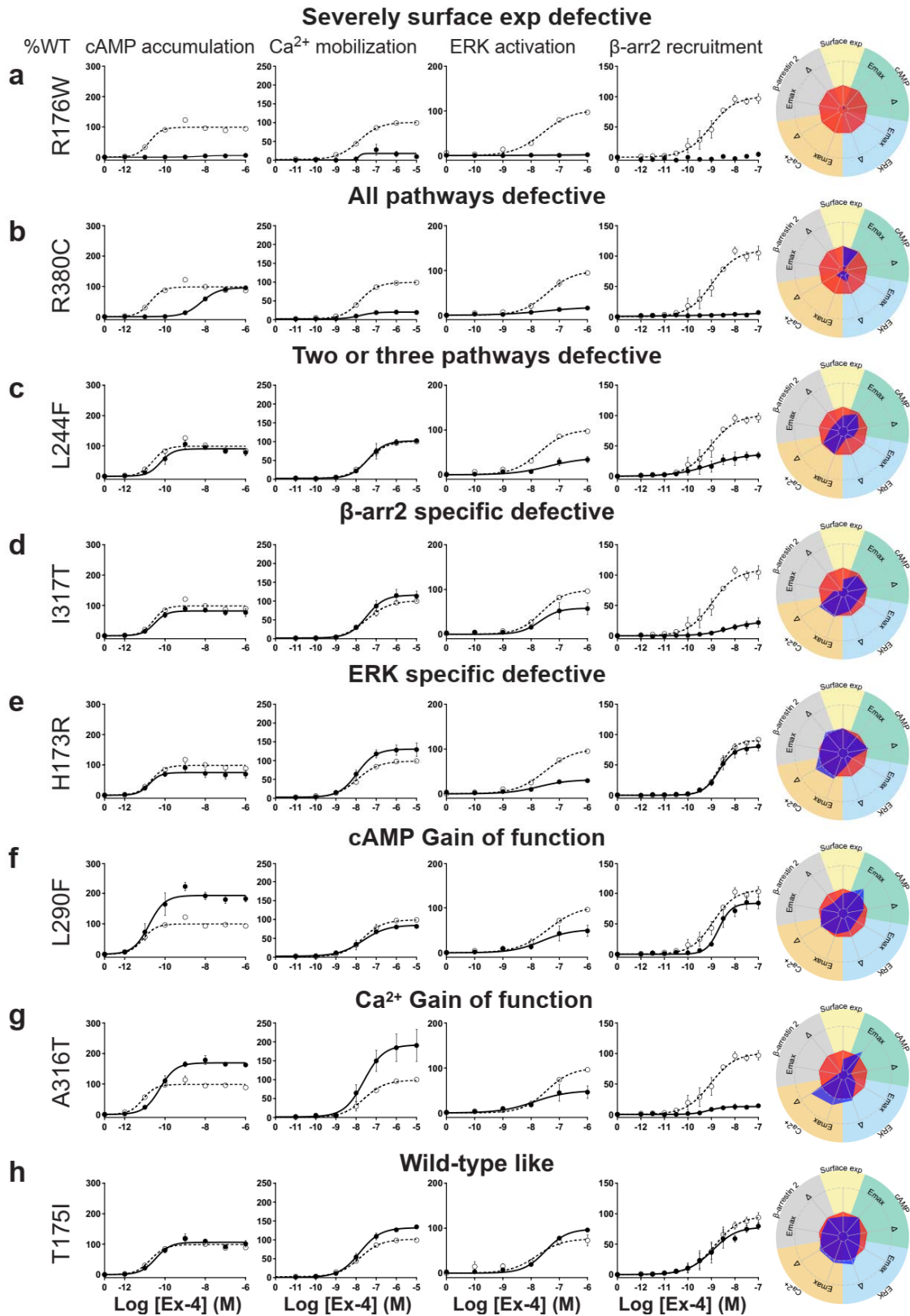
-
- 726 23. Bueno AB, *et al.* Structural insights into probe-dependent positive allosterism of the
727 GLP-1 receptor. *Nat Chem Biol* **16**, 1105-1110 (2020).
- 728
729 24. Jones B. The therapeutic potential of GLP-1 receptor biased agonism. *Br J Pharmacol*
730 **179**, 492-510 (2022).
- 731
732 25. Sonoda N, Imamura T, Yoshizaki T, Babendure JL, Lu JC, Olefsky JM. Beta-Arrestin-1
733 mediates glucagon-like peptide-1 signaling to insulin secretion in cultured pancreatic
734 beta cells. *Proc Natl Acad Sci U S A* **105**, 6614-6619 (2008).
- 735
736 26. Quoyer J, *et al.* GLP-1 mediates antiapoptotic effect by phosphorylating Bad through
737 a beta-arrestin 1-mediated ERK1/2 activation in pancreatic beta-cells. *J Biol Chem*
738 **285**, 1989-2002 (2010).
- 739
740 27. Schonegge AM, *et al.* Evolutionary action and structural basis of the allosteric switch
741 controlling beta(2)AR functional selectivity. *Nat Commun* **8**, 2169 (2017).
- 742
743 28. Lima-Fernandes E, *et al.* Distinct functional outputs of PTEN signalling are controlled
744 by dynamic association with beta-arrestins. *EMBO J* **30**, 2557-2568 (2011).
- 745
746 29. Berthault C, Staels W, Scharfmann R. Purification of pancreatic endocrine subsets
747 reveals increased iron metabolism in beta cells. *Mol Metab* **42**, 101060 (2020).
- 748
749 30. Guillaume JL, *et al.* The PDZ protein mupp1 promotes Gi coupling and signaling of
750 the Mt1 melatonin receptor. *J Biol Chem* **283**, 16762-16771 (2008).
- 751
752 31. Chen M, *et al.* Melatonin MT(1) and MT(2) receptor ERK signaling is differentially
753 dependent on G(i/o) and G(q/11) proteins. *J Pineal Res* **68**, e12641 (2020).
- 754
755 32. Kenakin T. New concepts in pharmacological efficacy at 7TM receptors: IUPHAR
756 review 2. *Br J Pharmacol* **168**, 554-575 (2013).
- 757
758 33. Cecon E, Oishi A, Jockers R. Melatonin receptors: molecular pharmacology and
759 signalling in the context of system bias. *Br J Pharmacol* **175**, 3263-3280 (2018).
- 760
761
762

763 **Figure 1**

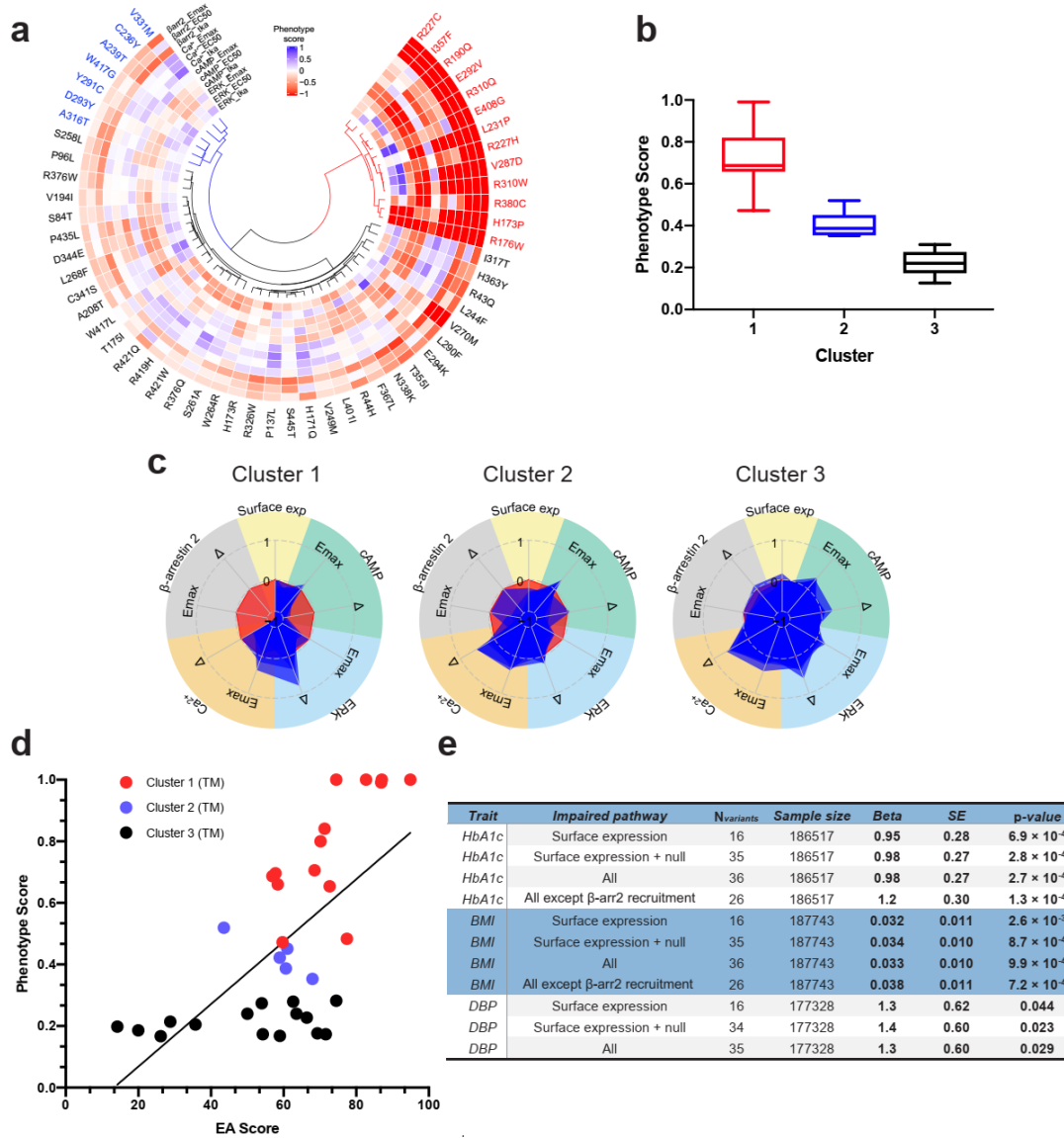


764

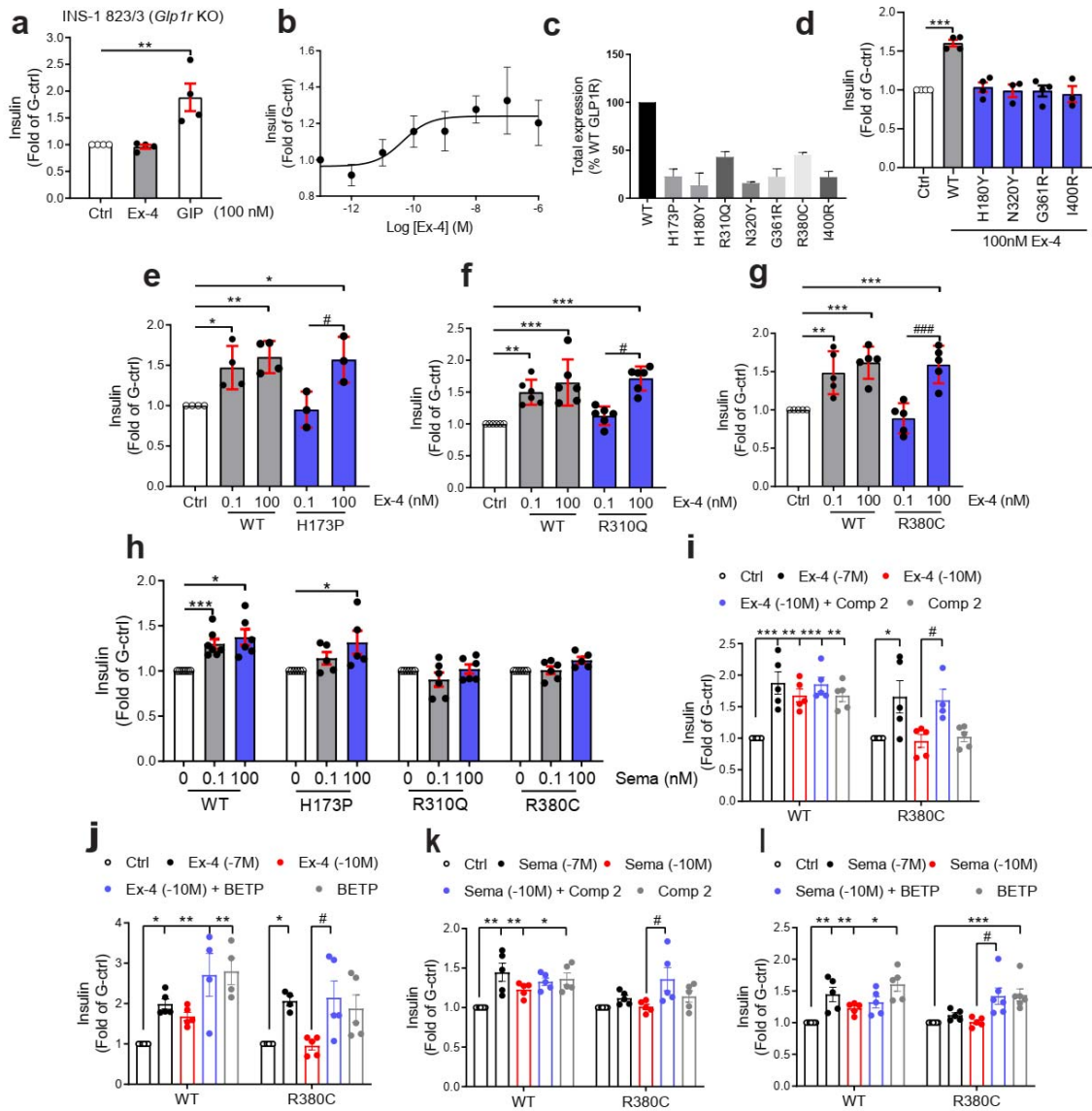
765

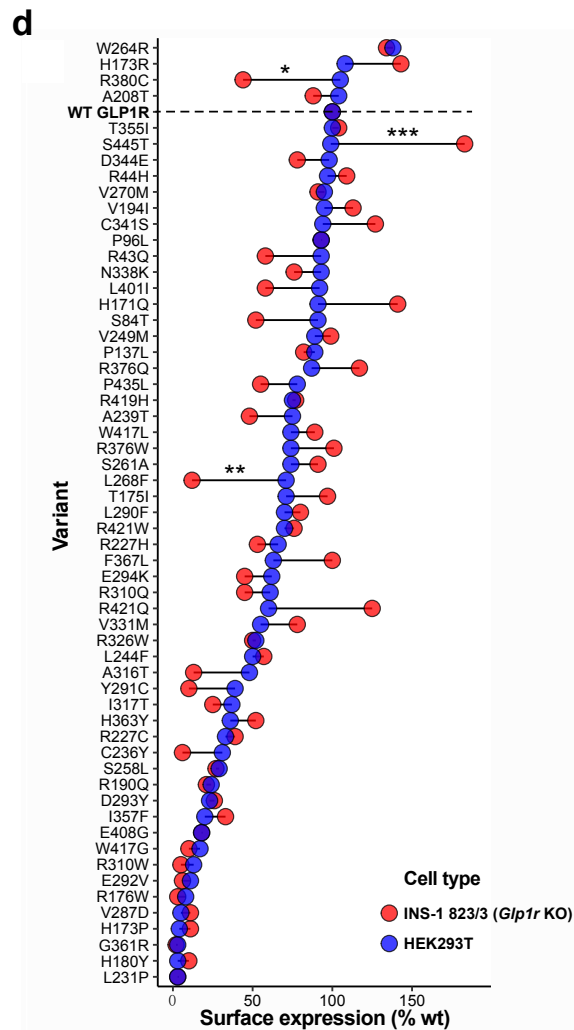
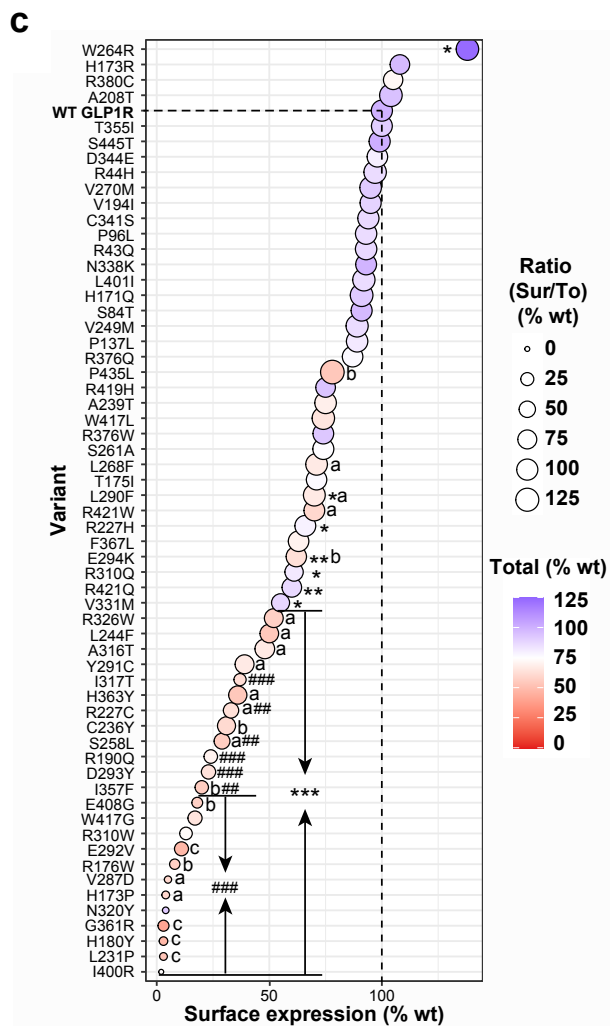
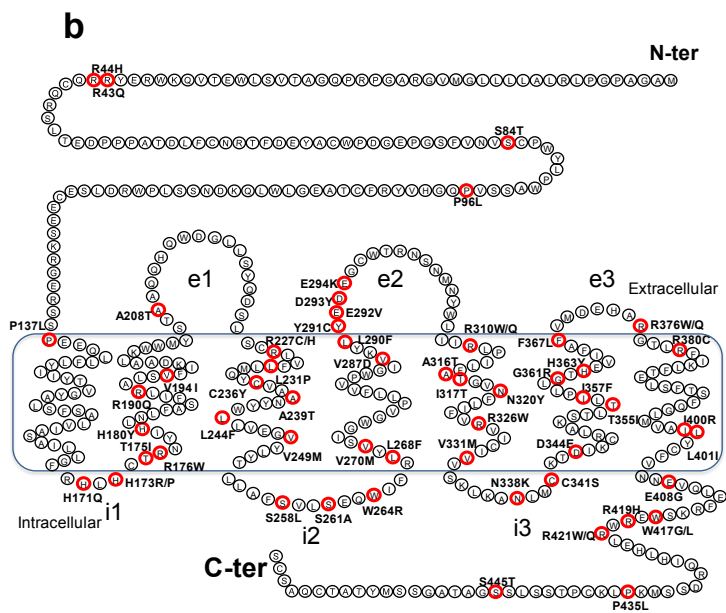
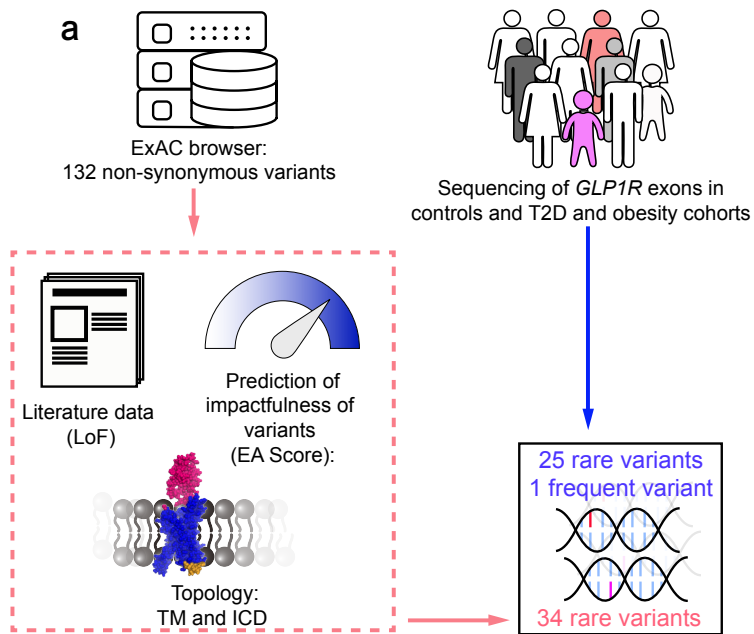


768 **Figure 3**

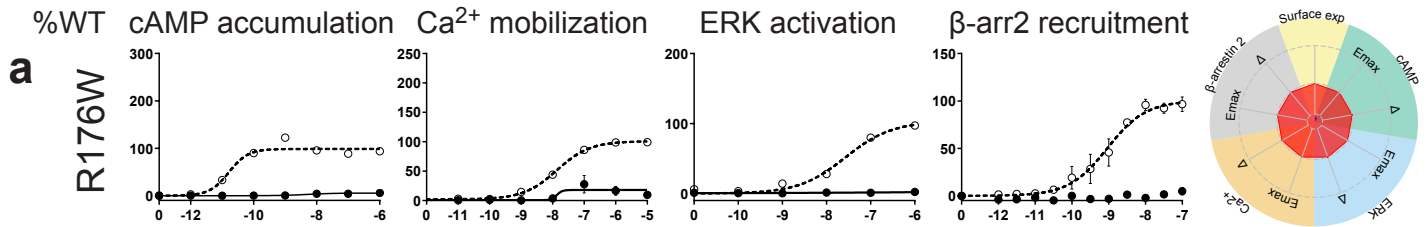


769

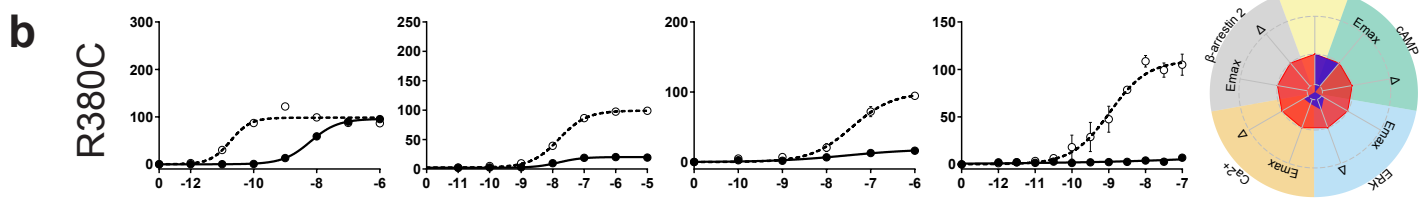




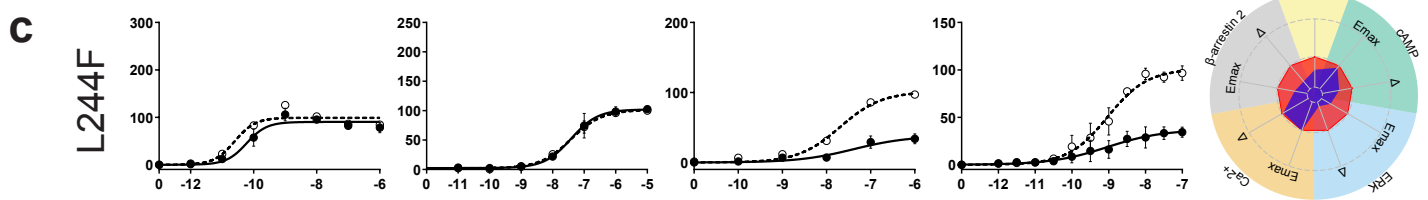
Severely surface exp defective



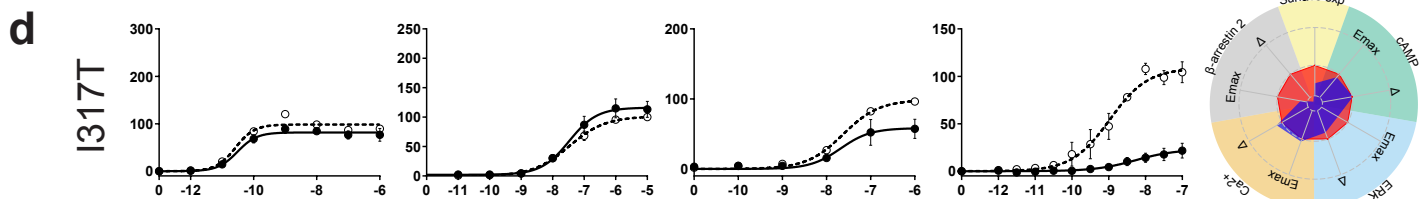
All pathways defective



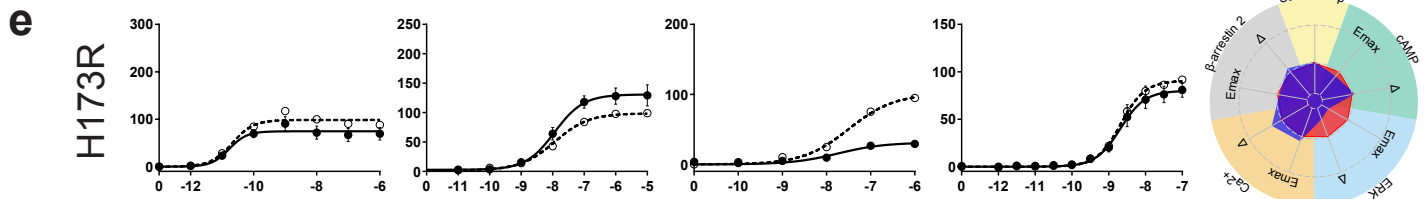
Two or three pathways defective



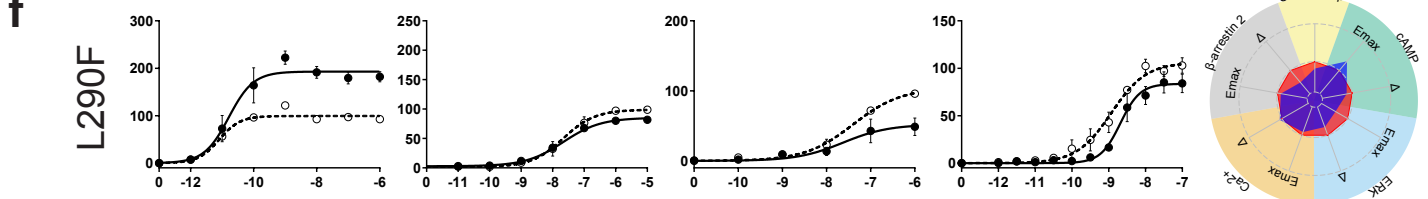
β -arr2 specific defective



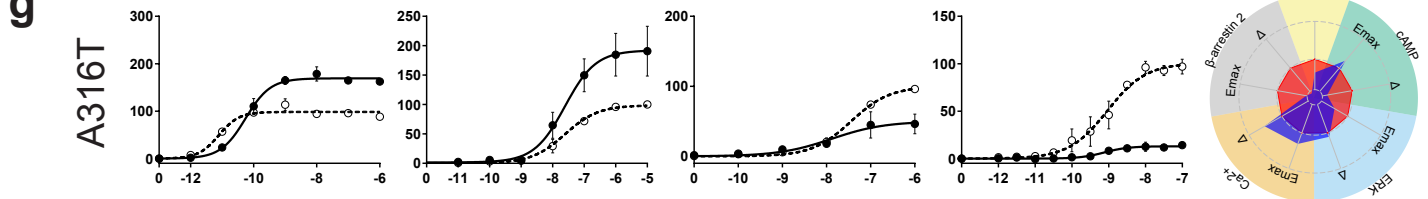
ERK specific defective



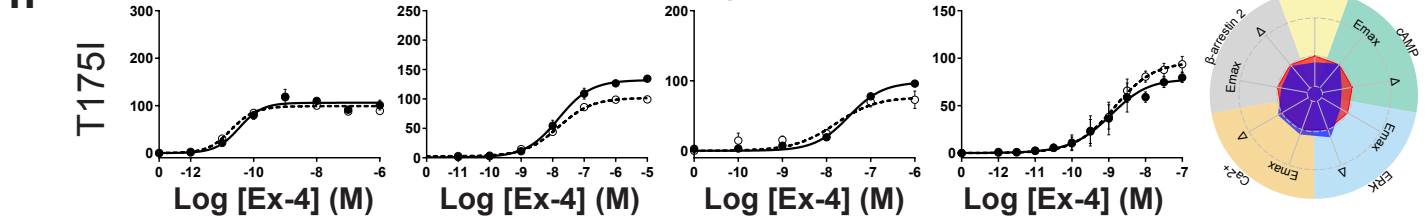
cAMP Gain of function

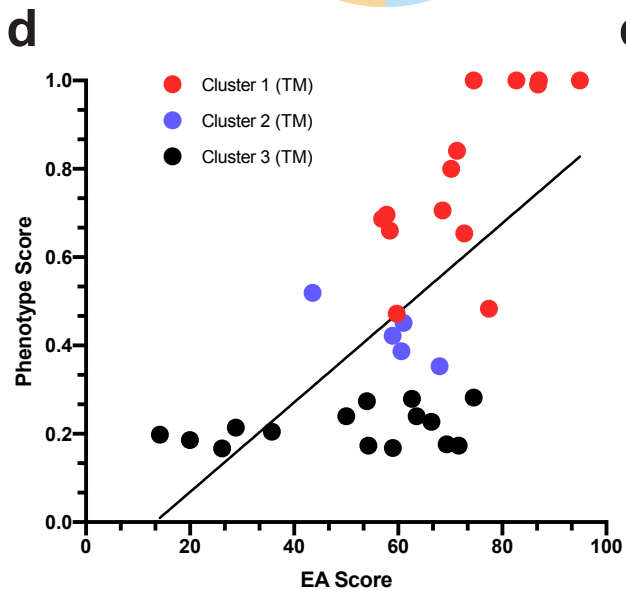
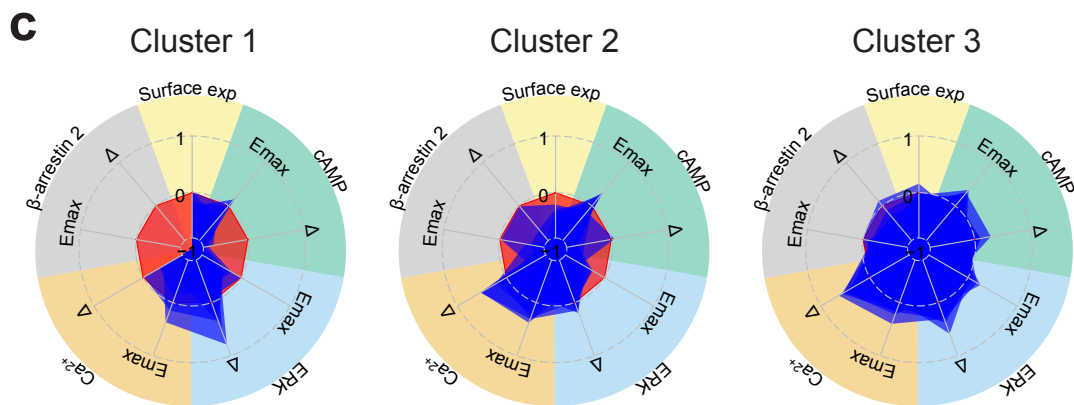
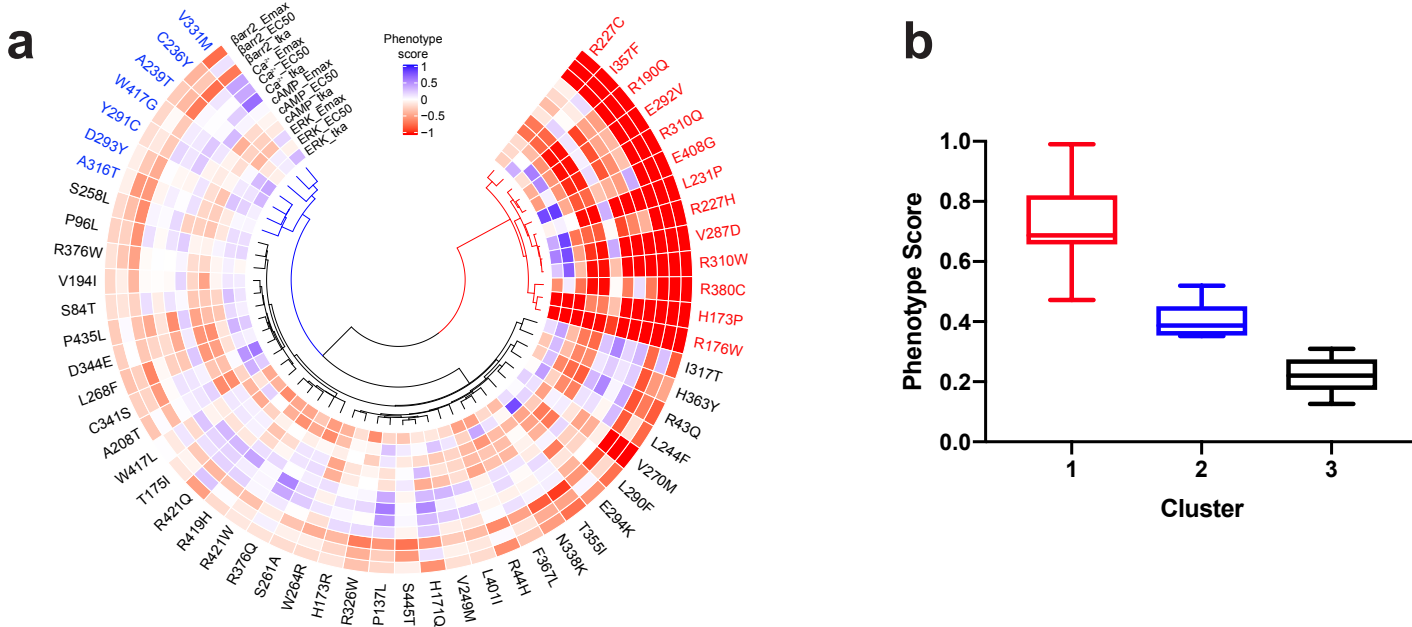


Ca²⁺ Gain of function



Wild-type like





e

Trait	Impaired pathway	N _{variants}	Sample size	Beta	SE	p-value
<i>Hba1c</i>	Surface expression	16	186517	0.95	0.28	6.9×10^{-4}
<i>Hba1c</i>	Surface expression + null	35	186517	0.98	0.27	2.8×10^{-4}
<i>Hba1c</i>	All	36	186517	0.98	0.27	2.7×10^{-4}
<i>Hba1c</i>	All except β-arr2 recruitment	26	186517	1.2	0.30	1.3×10^{-4}
<i>BMI</i>	Surface expression	16	187743	0.032	0.011	2.6×10^{-3}
<i>BMI</i>	Surface expression + null	35	187743	0.034	0.010	8.7×10^{-4}
<i>BMI</i>	All	36	187743	0.033	0.010	9.9×10^{-4}
<i>BMI</i>	All except β-arr2 recruitment	26	187743	0.038	0.011	7.2×10^{-4}
<i>DBP</i>	Surface expression	16	177328	1.3	0.62	0.044
<i>DBP</i>	Surface expression + null	34	177328	1.4	0.60	0.023
<i>DBP</i>	All	35	177328	1.3	0.60	0.029

